Eur. Phys. J. C 2, 597–606 (1998)
DOI 10.1007/s100529800838

THE EUROPEAN PHYSICAL JOURNAL C
© Springer-Verlag 1998

Measurement of triple gauge boson couplings from W^+W^- production at $\sqrt{s} = 172\text{GeV}$

The OPAL Collaboration

K. Ackerstaff[8], G. Alexander[23], J. Allison[16], N. Altekamp[5], K.J. Anderson[9], S. Anderson[12], S. Arcelli[2], S. Asai[24], D. Axen[29], G. Azuelos[18,a], A.H. Ball[17], E. Barberio[8], R.J. Barlow[16], R. Bartoldus[3], J.R. Batley[5], S. Baumann[3], J. Bechtluft[14], C. Beeston[16], T. Behnke[8], A.N. Bell[1], K.W. Bell[20], G. Bella[23], S. Bentvelsen[8], S. Bethke[14], O. Biebel[14], A. Biguzzi[5], S.D. Bird[16], V. Blobel[27], I.J. Bloodworth[1], J.E. Bloomer[1], M. Bobinski[10], P. Bock[11], D. Bonacorsi[2], M. Boutemeur[34], B.T. Bouwens[12], S. Braibant[12], L. Brigliadori[2], R.M. Brown[20], H.J. Burckhart[8], C. Burgard[8], R. Bürgin[10], P. Capiluppi[2], R.K. Carnegie[6], A.A. Carter[13], J.R. Carter[5], C.Y. Chang[17], D.G. Charlton[1,b], D. Chrisman[4], P.E.L. Clarke[15], I. Cohen[23], J.E. Conboy[15], O.C. Cooke[8], M. Cuffiani[2], S. Dado[22], C. Dallapiccola[17], G.M. Dallavalle[2], R. Davis[30], S. De Jong[12], L.A. del Pozo[4], K. Desch[3], B. Dienes[33,d], M.S. Dixit[7], E. do Couto e Silva[12], M. Doucet[18], E. Duchovni[26], G. Duckeck[34], I.P. Duerdoth[16], D. Eatough[16], J.E.G. Edwards[16], P.G. Estabrooks[6], H.G. Evans[9], M. Evans[13], F. Fabbri[2], M. Fanti[2], A.A. Faust[30], F. Fiedler[27], M. Fierro[2], H.M. Fischer[3], I. Fleck[8], R. Folman[26], D.G. Fong[17], M. Foucher[17], A. Fürtjes[8], D.I. Futyan[16], P. Gagnon[7], J.W. Gary[4], J. Gascon[18], S.M. Gascon-Shotkin[17], N.I. Geddes[20], C. Geich-Gimbel[3], T. Geralis[20], G. Giacomelli[2], P. Giacomelli[4], R. Giacomelli[2], V. Gibson[5], W.R. Gibson[13], D.M. Gingrich[30,a], D. Glenzinski[9], J. Goldberg[22], M.J. Goodrick[5], W. Gorn[4], C. Grandi[2], E. Gross[26], J. Grunhaus[23], M. Gruwé[8], C. Hajdu[32], G.G. Hanson[12], M. Hansroul[8], M. Hapke[13], C.K. Hargrove[7], P.A. Hart[9], C. Hartmann[3], M. Hauschild[8], C.M. Hawkes[5], R. Hawkings[27], R.J. Hemingway[6], M. Herndon[17], G. Herten[10], R.D. Heuer[8], M.D. Hildreth[8], J.C. Hill[5], S.J. Hillier[1], P.R. Hobson[25], R.J. Homer[1], A.K. Honma[28,a], D. Horváth[32,c], K.R. Hossain[30], R. Howard[29], P. Hüntemeyer[27], D.E. Hutchcroft[5], P. Igo-Kemenes[11], D.C. Imrie[25], M.R. Ingram[16], K. Ishii[24], A. Jawahery[17], P.W. Jeffreys[20], H. Jeremie[18], M. Jimack[1], A. Joly[18], C.R. Jones[5], G. Jones[16], M. Jones[6], U. Jost[11], P. Jovanovic[1], T.R. Junk[8], D. Karlen[6], V. Kartvelishvili[16], K. Kawagoe[24], T. Kawamoto[24], P.I. Kayal[30], R.K. Keeler[28], R.G. Kellogg[17], B.W. Kennedy[20], J. Kirk[29], A. Klier[26], S. Kluth[8], T. Kobayashi[24], M. Kobel[10], D.S. Koetke[6], T.P. Kokott[3], M. Kolrep[10], S. Komamiya[24], T. Kress[11], P. Krieger[6], J. von Krogh[11], P. Kyberd[13], G.D. Lafferty[16], R. Lahmann[17], W.P. Lai[19], D. Lanske[14], J. Lauber[15], S.R. Lautenschlager[31], J.G. Layter[4], D. Lazic[22], A.M. Lee[31], E. Lefebvre[18], D. Lellouch[26], J. Letts[12], L. Levinson[26], S.L. Lloyd[13], F.K. Loebinger[16], G.D. Long[28], M.J. Losty[7], J. Ludwig[10], A. Macchiolo[2], A. Macpherson[30], M. Mannelli[8], S. Marcellini[2], C. Markus[3], A.J. Martin[13], J.P. Martin[18], G. Martinez[17], T. Mashimo[24], P. Mättig[3], W.J. McDonald[30], J. McKenna[29], E.A. Mckigney[15], T.J. McMahon[1], R.A. McPherson[8], F. Meijers[8], S. Menke[3], F.S. Merritt[9], H. Mes[7], J. Meyer[27], A. Michelini[2], G. Mikenberg[26], D.J. Miller[15], A. Mincer[22,e], R. Mir[26], W. Mohr[10], A. Montanari[2], T. Mori[24], M. Morii[24], U. Müller[3], S. Mihara[24], K. Nagai[26], I. Nakamura[24], H.A. Neal[8], B. Nellen[3], R. Nisius[8], S.W. O'Neale[1], F.G. Oakham[7], F. Odorici[2], H.O. Ogren[12], A. Oh[27], N.J. Oldershaw[16], M.J. Oreglia[9], S. Orito[24], J. Pálinkás[33,d], G. Pásztor[32], J.R. Pater[16], G.N. Patrick[20], J. Patt[10], M.J. Pearce[1], R. Perez-Ochoa[8], S. Petzold[27], P. Pfeifenschneider[14], J.E. Pilcher[9], J. Pinfold[30], D.E. Plane[8], P. Poffenberger[28], B. Poli[2], A. Posthaus[3], D.L. Rees[1], D. Rigby[1], S. Robertson[28], S.A. Robins[22], N. Rodning[30], J.M. Roney[28], A. Rooke[15], E. Ros[8], A.M. Rossi[2], P. Routenburg[30], Y. Rozen[22], K. Runge[10], O. Runolfsson[8], U. Ruppel[14], D.R. Rust[12], R. Rylko[25], K. Sachs[10], T. Saeki[24], E.K.G. Sarkisyan[23], C. Sbarra[29], A.D. Schaile[34], O. Schaile[34], F. Scharf[3], P. Scharff-Hansen[8], P. Schenk[34], J. Schieck[11], P. Schleper[11], B. Schmitt[8], S. Schmitt[11], A. Schöning[8], M. Schröder[8], H.C. Schultz-Coulon[10], M. Schumacher[3], C. Schwick[8], W.G. Scott[20], T.G. Shears[16], B.C. Shen[4], C.H. Shepherd-Themistocleous[8], P. Sherwood[15], G.P. Siroli[2], A. Sittler[27], A. Skillman[15], A. Skuja[17], A.M. Smith[8], G.A. Snow[17], R. Sobie[28], S. Söldner-Rembold[10], R.W. Springer[30], M. Sproston[20], K. Stephens[16], J. Steuerer[27], B. Stockhausen[3], K. Stoll[10], D. Strom[19], P. Szymanski[20], R. Tafirout[18], S.D. Talbot[1], S. Tanaka[24], P. Taras[18], S. Tarem[22], R. Teuscher[8], M. Thiergen[10], M.A. Thomson[8], E. von Törne[3], S. Towers[6], I. Trigger[18], Z. Trócsányi[33], E. Tsur[23], A.S. Turcot[9], M.F. Turner-Watson[8], P. Utzat[11], R. Van Kooten[12], M. Verzocchi[10], P. Vikas[18], E.H. Vokurka[16], H. Voss[3], F. Wäckerle[10], A. Wagner[27], C.P. Ward[5], D.R. Ward[5], P.M. Watkins[1], A.T. Watson[1], N.K. Watson[1], P.S. Wells[8], N. Wermes[3], J.S. White[28], B. Wilkens[10], G.W. Wilson[27], J.A. Wilson[1], G. Wolf[26], T.R. Wyatt[16], S. Yamashita[24], G. Yekutieli[26], V. Zacek[18], D. Zer-Zion[8]

[1] School of Physics and Space Research, University of Birmingham, Birmingham B15 2TT, UK
[2] Dipartimento di Fisica dell' Università di Bologna and INFN, I-40126 Bologna, Italy
[3] Physikalisches Institut, Universität Bonn, D-53115 Bonn, Germany
[4] Department of Physics, University of California, Riverside CA 92521, USA

[5] Cavendish Laboratory, Cambridge CB3 0HE, UK
[6] Ottawa-Carleton Institute for Physics, Department of Physics, Carleton University, Ottawa, Ontario K1S 5B6, Canada
[7] Centre for Research in Particle Physics, Carleton University, Ottawa, Ontario K1S 5B6, Canada
[8] CERN, European Organisation for Particle Physics, CH-1211 Geneva 23, Switzerland
[9] Enrico Fermi Institute and Department of Physics, University of Chicago, Chicago IL 60637, USA
[10] Fakultät für Physik, Albert Ludwigs Universität, D-79104 Freiburg, Germany
[11] Physikalisches Institut, Universität Heidelberg, D-69120 Heidelberg, Germany
[12] Indiana University, Department of Physics, Swain Hall West 117, Bloomington IN 47405, USA
[13] Queen Mary and Westfield College, University of London, London E1 4NS, UK
[14] Technische Hochschule Aachen, III Physikalisches Institut, Sommerfeldstrasse 26-28, D-52056 Aachen, Germany
[15] University College London, London WC1E 6BT, UK
[16] Department of Physics, Schuster Laboratory, The University, Manchester M13 9PL, UK
[17] Department of Physics, University of Maryland, College Park, MD 20742, USA
[18] Laboratoire de Physique Nucléaire, Université de Montréal, Montréal, Quebec H3C 3J7, Canada
[19] University of Oregon, Department of Physics, Eugene OR 97403, USA
[20] Rutherford Appleton Laboratory, Chilton, Didcot, Oxfordshire OX11 0QX, UK
[22] Department of Physics, Technion-Israel Institute of Technology, Haifa 32000, Israel
[23] Department of Physics and Astronomy, Tel Aviv University, Tel Aviv 69978, Israel
[24] International Centre for Elementary Particle Physics and Department of Physics, University of Tokyo, Tokyo 113, and Kobe University, Kobe 657, Japan
[25] Brunel University, Uxbridge, Middlesex UB8 3PH, UK
[26] Particle Physics Department, Weizmann Institute of Science, Rehovot 76100, Israel
[27] Universität Hamburg/DESY, II Institut für Experimental Physik, Notkestrasse 85, D-22607 Hamburg, Germany
[28] University of Victoria, Department of Physics, P O Box 3055, Victoria BC V8W 3P6, Canada
[29] University of British Columbia, Department of Physics, Vancouver BC V6T 1Z1, Canada
[30] University of Alberta, Department of Physics, Edmonton AB T6G 2J1, Canada
[31] Duke University, Department of Physics, Durham, NC 27708-0305, USA
[32] Research Institute for Particle and Nuclear Physics, H-1525 Budapest, P O Box 49, Hungary
[33] Institute of Nuclear Research, H-4001 Debrecen, P O Box 51, Hungary
[34] Ludwigs-Maximilians-Universität München, Sektion Physik, Am Coulombwall 1, D-85748 Garching, Germany

Received: 16 September 1997 / Published online: 30 March 1998

Abstract. We present measurements of triple gauge boson coupling parameters using data recorded by the OPAL detector at LEP2 at a centre-of-mass energy of 172 GeV. A total of 120 W-pair candidates has been selected in the $q\bar{q}q\bar{q}$, $q\bar{q}\ell\overline{\nu}_\ell$ and $\ell\overline{\nu}_\ell\overline{\ell}'\nu_{\ell'}$ decay channels, for an integrated luminosity of $10.4\,\mathrm{pb}^{-1}$. We use these data to determine several different anomalous coupling parameters using the measured cross-section and the distributions of kinematic variables. We measure $\alpha_{B\phi}$=$0.35^{+1.29}_{-1.07} \pm 0.38$, $\alpha_{W\phi}$=$0.00^{+0.30}_{-0.28} \pm 0.11$, $\alpha_W = 0.18^{+0.49}_{-0.47} \pm 0.23$, Δg_1^z=$-0.03^{+0.40}_{-0.37} \pm 0.14$, $\Delta\kappa_\gamma^{(HISZ)} = 0.03^{+0.55}_{-0.51} \pm 0.20$, and $\Delta\kappa$=$0.03^{+0.49}_{-0.46} \pm 0.21$. Combining the $\alpha_{W\phi}$ result with our previous result obtained from the 161 GeV data sample we measure $\alpha_{W\phi}$=$-0.08^{+0.28}_{-0.25} \pm 0.10$. All of these measurements are consistent with the Standard Model.

1 Introduction

During the initial year of operation of LEP2, centre-of-mass energies have been attained which allow the production of W^+W^- boson pairs for the first time in e^+e^- collisions. A total integrated luminosity of 9.9 pb^{-1} was recorded at a centre-of-mass energy of 161 GeV and $10.4\,pb^{-1}$ at 172 GeV.

The W^+W^- production process involves the triple gauge boson vertices between the W^+W^- and the Z^0 or photon. The measurement of these triple gauge boson couplings (TGCs) and the search for possible anomalous values is one of the principal physics goals at LEP2. Previous direct measurements have been presented by CDF [1] and D0 [2], and by the LEP experiments using the 161 GeV[3, 4] and 172 GeV[5] data. In this paper we present an analysis of the 172 GeV data sample to make measurements of several anomalous coupling parameters. We also combine these results with the measurement obtained from our 161 GeV data sample [3].

The observable effects of possible deviations from the Standard Model have been studied extensively [6]. Anomalous TGCs can affect both the total production cross-section and the shape of the differential cross-section as a function of the W^- production angle. Additionally, the relative contributions of each helicity state of the W bosons are changed, which in turn affects the distributions of their decay products. In this analysis we make use of both

[a] and at TRIUMF, Vancouver, Canada V6T 2A3
[b] and Royal Society University Research Fellow
[c] and Institute of Nuclear Research, Debrecen, Hungary
[d] and Department of Experimental Physics, Lajos Kossuth University, Debrecen, Hungary
[e] and Department of Physics, New York University, NY 1003, USA

production rate and angular distributions measured using events where the W boson pair decays to the $q\bar{q}\ell\bar{\nu}_\ell$ channel (hereafter $q\bar{q}\ell\bar{\nu}_\ell$ also refers to the charge conjugate state). We also use the measured production rate for events where the W boson pair decays to the $q\bar{q}q\bar{q}$ and $\ell\bar{\nu}_\ell\bar{\ell}'\nu_{\ell'}$ channels.

Anomalous coupling parameters

The most general Lorentz invariant Lagrangian [6–9] which describes the triple gauge boson interaction has fourteen independent terms, seven describing the WWγ vertex and seven describing the WWZ vertex. This parameter space is very large, and it is not currently possible to measure all fourteen couplings independently. Assuming electromagnetic gauge invariance and C and P conservation the number of parameters reduces to five, which can be taken as $g_1^z, \kappa_z, \kappa_\gamma, \lambda_z$ and λ_γ [6,7]. In the Standard Model $g_1^z = \kappa_z = \kappa_\gamma = 1$ and $\lambda_z = \lambda_\gamma = 0$.

Different sets of parameters have also been proposed which are motivated by SU(2)×U(1) gauge invariance and constraints arising from precise measurements at LEP1. One such set proposes three independent linear combinations of the couplings [6,8] which are not tightly constrained [10,11] by existing LEP1 data. These are:

$$\alpha_{B\phi} \equiv \Delta\kappa_\gamma - \Delta g_1^z \cos^2\theta_w \quad (1)$$

$$\alpha_{W\phi} \equiv \Delta g_1^z \cos^2\theta_w \quad (2)$$

$$\alpha_W \equiv \lambda_\gamma. \quad (3)$$

with the constraints that $\Delta\kappa_z = -\Delta\kappa_\gamma \tan^2\theta_w + \Delta g_1^z$ and $\lambda_z = \lambda_\gamma$. The Δ indicates the deviation of the respective quantity from its Standard Model value and θ_w is the weak mixing angle. Each of the α parameters has the value zero in the Standard Model. A similar approach, HISZ [11], reduces this set to two parameters with the extra constraint $\alpha_{B\phi} = \alpha_{W\phi}$. This extra constraint is equivalent to $\Delta g_1^z = \Delta\kappa_\gamma/(2\cos^2\theta_w)$, and $\Delta\kappa_\gamma$ and $\lambda_\gamma \equiv \alpha_W$ are normally used as the variable parameters.

In this analysis, we present measurements of the following parameters:

- $\alpha_{B\phi}$, $\alpha_{W\phi}$ and α_W,
- the two and three dimensional correlations of $\alpha_{B\phi}$, $\alpha_{W\phi}$ and α_W,
- Δg_1^z and the two dimensional correlation of Δg_1^z and α_W,
- $\Delta\kappa_\gamma$ assuming the HISZ constraints, and the two dimensional correlation of $\Delta\kappa_\gamma$ and α_W,
- $\Delta\kappa$ assuming $\Delta\kappa_z = \Delta\kappa_\gamma$, and the two dimensional correlation of $\Delta\kappa$ and α_W.

In each case, all parameters not mentioned explicitly are set to their Standard Model values. The measurements of $\Delta\kappa_\gamma$ and $\Delta\kappa$ are included to facilitate comparisons with results from the CDF and D0 collaborations.

2 Data selection and reconstruction

The data were recorded at an average centre-of-mass energy [12] of $\sqrt{s} = 172.12 \pm 0.06$ GeV using the OPAL detector, which is fully described elsewhere [13,14]. A total integrated luminosity of $10.36 \pm 0.06\,\mathrm{pb}^{-1}$ was recorded at this energy. Events are selected corresponding to different W pair decay combinations. These are: (i) $q\bar{q}q\bar{q}$ events where both W bosons decay to a quark-antiquark final state, (ii) $q\bar{q}\ell\bar{\nu}_\ell$ events where one W decays to a quark-antiquark final state, and the other W decays to an electron, muon or tau, plus a neutrino and (iii) $\ell\bar{\nu}_\ell\bar{\ell}'\nu_{\ell'}$ events where both W bosons decay leptonically.

The selection procedures which have been developed for these channels are based upon a multivariate likelihood method. These procedures are described fully in [15] and the results presented there are summarised in Table 1. In this analysis we use all of the efficiencies, background and systematic error evaluations exactly as presented in [15] to determine the constraint upon anomalous couplings arising from the observed event rate.

We also constrain anomalous couplings using the production and decay angular distributions in the $q\bar{q}\ell\bar{\nu}_\ell$ channels. We choose to use only these channels as they are the most straightforward to reconstruct and there is no ambiguity in assigning decay fermion pairs to each W, nor in determining the charge of each W through the decay lepton charge. For this part of the analysis we make additional requirements to those described in [15] in order to ensure that the charged lepton is well identified and to further reduce background contamination. In the following we describe the reconstruction of $q\bar{q}\ell\bar{\nu}_\ell$ events used for the angular distribution analysis and the extra selection requirements and the corresponding reevaluation of the backgrounds.

All Monte Carlo samples which are used are generated assuming the current central value of the world average W boson mass of $M_W = 80.33 \pm 0.15$ GeV [16]. The total W^+W^- cross section is assumed to be 12.4 pb as obtained from the GENTLE [17] program. All Monte Carlo samples used are passed through the full OPAL simulation program [18] and then subjected to the same reconstruction procedures as applied to the data.

2.1 $q\bar{q}e\bar{\nu}_e$ and $q\bar{q}\mu\bar{\nu}_\mu$ events

The $q\bar{q}e\bar{\nu}_e$ and $q\bar{q}\mu\bar{\nu}_\mu$ events are characterised by two well-separated hadronic jets, a high momentum charged lepton and missing momentum from the unobserved neutrino. The selections described in [15] result in a single track being identified as the most likely lepton candidate. The electron momentum is constructed from the direction measured by the tracking detectors and the energy measured in the electromagnetic calorimeters. In the case of muons, the momentum measured using the tracking detectors is used. The remaining tracks and calorimeter clusters in the event are grouped into two jets using the $k_\perp$ algorithm [19]. The total energy and momentum of each of the jets are calculated using both tracks and electromagnetic clusters using the method of [20]. The main residual background is from misidentified $q\bar{q}\tau\bar{\nu}_\tau$ events. We reduce this further by demanding $M_{\ell\nu} > 50$ GeV, where $M_{\ell\nu}$ is the invariant mass constructed from the lepton four-momentum and the missing three-momentum assuming a

Table 1. Observed number of candidate events in each W^+W^- decay channel, together with expected numbers of signal and background events predicted by the Standard Model. The predicted numbers for signal include systematic uncertainties from the efficiency, luminosity, beam energy, W^+W^- cross-section and M_W, while the background estimates include selection and luminosity uncertainties. (Note: In this table, contamination in the $q\bar{q}\ell\overline{\nu}_\ell$ channels from other $q\bar{q}\ell\overline{\nu}_\ell$ channels is listed separately, whereas in [15] it is included in the signal.)

Channel	Expected Signal	$q\bar{q}\ell\overline{\nu}_\ell$ Bkg.	Other Bkg.	Total	Observed
From [15] [see note in caption].					
$W^+W^- \to q\bar{q}e\overline{\nu}_e$	16.2 ± 0.4	0.6 ± 0.0	1.2 ± 0.4	18.0 ± 0.6	19
$W^+W^- \to q\bar{q}\mu\overline{\nu}_\mu$	16.5 ± 0.4	0.9 ± 0.0	0.6 ± 0.1	17.9 ± 0.4	16
$W^+W^- \to q\bar{q}\tau\overline{\nu}_\tau$	11.6 ± 0.4	1.9 ± 0.1	2.7 ± 0.7	16.2 ± 0.8	20
$W^+W^- \to q\bar{q}q\bar{q}$	46.8 ± 1.2	–	14.3 ± 2.9	61.0 ± 3.1	57
$W^+W^- \to \ell\overline{\nu}_\ell\overline{\ell}'\nu_{\ell'}$	10.7 ± 0.3	–	0.8 ± 0.2	11.5 ± 0.4	8
After additional requirements for angular distribution analysis.					
$W^+W^- \to q\bar{q}e\overline{\nu}_e$	16.0 ± 0.4	0.5 ± 0.0	0.6 ± 0.3	17.1 ± 0.5	17
$W^+W^- \to q\bar{q}\mu\overline{\nu}_\mu$	16.4 ± 0.4	0.6 ± 0.0	0.2 ± 0.3	17.2 ± 0.5	15
$W^+W^- \to q\bar{q}\tau\overline{\nu}_\tau$	9.8 ± 0.4	0.8 ± 0.1	1.6 ± 0.3	12.2 ± 0.5	16

Table 2. Signal and background cross sections for the $q\bar{q}e\overline{\nu}_e$, $q\bar{q}\mu\overline{\nu}_\mu$ and $q\bar{q}\tau\overline{\nu}_\tau$ samples used in the analysis of angular distributions. The errors on the expected signal include both statistical and systematic errors. The errors on the background estimations are statistical only

Source	Channel		
	$q\bar{q}e\overline{\nu}_e$	$q\bar{q}\mu\overline{\nu}_\mu$	$q\bar{q}\tau\overline{\nu}_\tau$
Expected signal (fb)	1543 ± 16	1579 ± 13	962 ± 19
Background (fb)			
$W^+W^- \to q\bar{q}e\overline{\nu}_e$	–	5 ± 1	37 ± 3
$W^+W^- \to q\bar{q}\mu\overline{\nu}_\mu$	0.8 ± 0.5	–	44 ± 4
$W^+W^- \to q\bar{q}\tau\overline{\nu}_\tau$	49 ± 4	59 ± 4	–
$W^+W^- \to q\bar{q}q\bar{q}$	0 ± 0	0.6 ± 0.4	8 ± 2
$W^+W^- \to \ell\overline{\nu}_\ell\overline{\ell}'\nu_{\ell'}$	0.8 ± 0.5	0.3 ± 0.3	0.6 ± 0.4
$Z^0/\gamma \to q\bar{q}$	22 ± 6	9 ± 4	43 ± 8
4-fermion (non-qqee)	-1 ± 25	15 ± 25	59 ± 20
4-fermion (qqee)	20 ± 11	0 ± 0	44 ± 20
Two-photon	22 ± 13	0 ± 0	0 ± 0
Total (fb)	113 ± 31	88 ± 25	236 ± 30
Total (%)	7 ± 2	6 ± 2	25 ± 3

zero mass. This extra requirement results in efficiencies of 85% and 87% for the electron and muon channels respectively, which is a loss of 0.5% in each channel with respect to [15]. The expected number of signal events and the number of events selected from the data are shown in Table 1. The values in this table correspond to an integrated luminosity of $10.36 \pm 0.06\,\mathrm{pb}^{-1}$ at 172.12 ± 0.06 GeV. Table 2 shows the signal and background cross sections used in the analysis of the angular distributions. The expected number of signal events is evaluated using PYTHIA [21] and is normalised such that the total cross section agrees with GENTLE.

2.2 $q\bar{q}\tau\overline{\nu}_\tau$ events

The signature of $q\bar{q}\tau\overline{\nu}_\tau$ events is less well defined than that of the electron or muon channels due to the presence of one or more additional neutrinos, and the absence of a high momentum lepton. The primary selection for this channel described in [15] results in the identification of the most likely one or three track tau decay candidate classified as an electron, muon, one-prong hadronic or three-prong hadronic decay. The remaining tracks and calorimeter clusters in the event are grouped into two jets as described above.

The ensuing analysis of this channel relies upon the correct tau decay products being identified in order that they give a reasonable approximation to the original tau flight direction, and that the direction of the hadronic W system can be reliably measured. We therefore make additional requirements. In the electron and muon decay channels we require the lepton momentum to be greater than 5 GeV. We demand that the track is separated from other activity in the detector by requiring that the angle between the lepton direction and both jet axes be greater than 20°. In the one-prong and three-prong hadronic decay channels we require the total momentum of the decay products to be greater than 11 GeV and the angle between the direction of the vector sum of the decay products and either jet axis to be greater than 20°. In addition we require the two hadronic jets to be back–to–back within 65°. These requirements result in a correct tau decay product identification of 97%, 96%, 90% and 89% in the electron, muon, one-prong hadronic and three-prong hadronic decay channels respectively, where the tau decay products are said to be correct if they lie within 10° of the original tau flight direction and have the correct charge. The overall selection efficiency drops from 61% to 53% with respect to [15]. The expected signal and the total number of events selected from the data are shown in Tables 1 and 2.

2.3 Backgrounds

The estimated background contaminations from different sources are given in Table 2. The main background process, $Z^0/\gamma \to q\bar{q}$, is simulated using PYTHIA. Most of the processes leading to four fermions in the final state are evaluated using grc4f [22] and EXCALIBUR [23]. Backgrounds from two-photon processes are evaluated using PYTHIA.

The background labelled in Table 2 as '4-fermion' represents the contribution due to all four fermion diagrams excluding the three main W^+W^- production diagrams (known as "CC03" [6]). This contribution includes all diagrams which lead to the same final state as the signal, and which may therefore interfere to give a negative contribution, as well as those leading to different final states but which can be misidentified as signal. The 4-fermion contamination is obtained using grc4f, by subtracting the accepted cross section for events generated using only the CC03 diagrams from that found for events generated using all diagrams. The results were found to be in good agreement with a similar study using EXCALIBUR.

3 Kinematic variables for the $q\bar{q}\ell\bar{\nu}_\ell$ event sample

For each $q\bar{q}\ell\bar{\nu}_\ell$ event we measure three angles[1] [6,8,24]:

1) $\cos\theta_W$, the production angle of the W^- with respect to the e^- beam direction,
2) $\cos\theta^*_\ell$, the polar angle of the charged lepton with respect to the parent W flight direction measured in the W rest frame,
3) ϕ^*_ℓ, the azimuthal angle of the charged lepton around the axis given by the parent W flight direction, measured in the W rest frame.

In the case of the $q\bar{q}e\bar{\nu}_e$ and $q\bar{q}\mu\bar{\nu}_\mu$ events we perform a three constraint kinematic fit, which demands energy and momentum conservation assuming a zero mass for the missing neutrino. The fit minimises a χ^2 sum which also includes a contribution from the difference between[2] the nominal world average W mass of 80.33 GeV and the fitted masses of both the hadronic and leptonic systems. We demand that the kinematic fit converges with a probability of $> 10^{-3}$. For the small number of approximately 5% of events which fail at this point we revert to using the results of a fit without the W mass constraints. We then obtain $\cos\theta_W$ by adding together the kinematically fitted four-momenta of the two jets. The charges of the W bosons are determined by the sign of the charged lepton. The decay angles are obtained from the fitted charged lepton four-momentum after boosting back to the parent W rest frame using the fitted W four-momentum to determine the boost.

In the case of the $q\bar{q}\tau\bar{\nu}_\tau$ events we obtain $\cos\theta_W$ by adding together the measured four-momenta of the two reconstructed jets, and the charges of the W bosons are determined by the sign of the sum of the charges of the tracks of the tau decay products. In order to reconstruct the decay angles, the flight direction of the tau is approximated by the direction of its charged decay products. The four unknown quantities can then be calculated using energy and momentum conservation. These are the energy of the tau and the three-momentum of the tau neutrino originating directly from the W decay. The decay angles are then obtained as for the other $q\bar{q}\ell\bar{\nu}_\ell$ events.

In Fig. 1 we show the distributions of all three angles obtained from the combined $q\bar{q}e\bar{\nu}_e$, $q\bar{q}\mu\bar{\nu}_\mu$ and $q\bar{q}\tau\bar{\nu}_\tau$ event sample, and the expected distributions for $\alpha_{W\phi} = \pm 2$ and 0. The shapes of the the distributions are obtained from fully simulated Monte Carlo event samples. The distributions are normalised to number of events observed in the data.

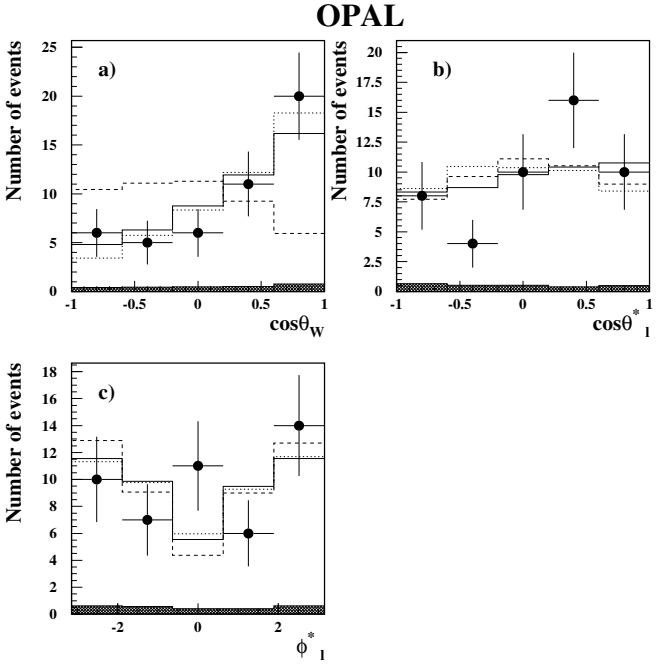

Fig. 1. The distributions of the kinematic variables $\cos\theta_W$, $\cos\theta^*_\ell$, ϕ^*_ℓ obtained from the $q\bar{q}\ell\bar{\nu}_\ell$ events. The *hatched histogram* shows the non-$q\bar{q}\ell\bar{\nu}_\ell$ background. These are compared with the distribution expected in the Standard Model using fully simulated Monte Carlo events. The predicted distributions for $\alpha_{W\phi} = +2(-2)$ are also shown as *dotted* (*dashed*) *lines*. Note: in the case of $W^+ \to \bar{\ell}\nu$ events the value of ϕ^*_ℓ is shifted by π in order to overlay W^+ and W^- distributions in the same plot

[1] The definition of the axes is such that z is along the parent W flight direction and y is in the direction $\mathbf{e}^- \times \mathbf{W}$ where $\mathbf{e}^-$ is the electron beam direction and $\mathbf{W}$ is the parent W flight direction. The axes are defined in the W rest frame

[2] The W mass is treated as Gaussian in the kinematic fit. However, in order to simulate the expected Breit-Wigner form of the W mass spectrum, the variance of the Gaussian is updated at each iteration of the kinematic fit in such a way that the probabilities of observing the current fitted W mass are equal whether calculated using the Gaussian distribution or using a simple Breit-Wigner

4 Anomalous coupling analysis

In this section we present the analysis of the W^+W^- event sample in order to place limits upon anomalous coupling parameters. The analysis uses the event sample in two distinct ways. The first part uses only the $q\bar{q}\ell\overline{\nu}_\ell$ events to constrain TGCs through the predicted variation of the differential distribution of the production and decay angles. We do not distinguish between the $q\bar{q}e\overline{\nu}_e$, $q\bar{q}\mu\overline{\nu}_\mu$ and $q\bar{q}\tau\overline{\nu}_\tau$ events. The second part uses all channels to constrain TGCs through the variation of the expected cross-section as a function of TGC parameter. A log likelihood, $\log L$, curve is calculated for each part of the analysis. These are independent and are added together to obtain a combined $\log L$ curve from which the results are obtained. In the following the symbol α stands for a generic anomalous coupling parameter.

A binned likelihood method is used to analyse the three dimensional differential cross section. We divide $\cos\theta_W$ into 20 bins in the range [−1,1], $\cos\theta^*_\ell$ into 10 bins in the range [−1,1] and ϕ^*_ℓ into 5 bins in the range $[-\pi, \pi]$. The resolutions of the variables are finer than the corresponding bin widths.

The $\log L$ distribution is obtained in several steps. In the first step we parameterise in each bin the expected cross-section due to W^+W^- production, before detector and acceptance effects, as a function of α. We denote this as $\sigma_i^{\rm gen}(\alpha)$, where i refers to each bin in the three dimensional space. It is obtained using large samples of EXCALIBUR Monte Carlo events including the effects of the W width, Γ_W, and initial state radiation, ISR, but without detector simulation. In each bin, $\sigma_i^{\rm gen}(\alpha)$ is parametrised using the fact that σ is a quadratic function of α (as α enters linearly in the Lagrangian). Several samples are generated for different values of α and a quadratic parameterisation obtained to predict $\sigma(\alpha)$ for all other values of α.

In the second step we calculate a correction matrix to include the effects of acceptance, resolution and feedthrough from other W^+W^- decay channels. We use fully simulated Monte Carlo events generated with $\alpha = 0$ to obtain factors, c_{ki}, which allow for events generated in true bin i being reconstructed in bin k. All W^+W^- decays which are reconstructed as $q\bar{q}\ell\overline{\nu}_\ell$ events in bin k are counted in the correction factors c_{ki}. The c_{ki} therefore include the effect of feedthrough from other W^+W^- decay channels which is always a fixed fraction of the signal which is independent of the value of α. For a given bin, corresponding to a limited phase space region, the c_{ki} factors are assumed to be independent of α. Possible biases due to this assumption are discussed in Sect. 5.

Combining these terms results in the expected observed cross-section for each bin k, due to all W^+W^- channels:

$$\sigma_k^{\rm WW}(\alpha) = \sum_i c_{ki}\sigma_i^{\rm gen}(\alpha)$$

In the next step the cross-section for the $Z^0/\gamma \to q\bar{q}$ and two photon backgrounds, $\sigma_k^{\rm bkg}$, is estimated using PYTHIA and is added to give $\sigma_k^{\rm all}(\alpha)$. The small background due to four fermion diagrams given in Table 2 is neglected. The effect of this neglect is discussed in Sect. 5. The quantity $\sigma_k^{\rm all}(\alpha)$ now contains all of the information on the shape of the expected distribution as a function of α. We multiply this by a scale factor to give the prediction for the number of events in each bin, n_k, where the scale factor is chosen such that the predicted total number of events is equal to the actual number of events observed in the data. This is to ensure that we do not incorporate any information from the overall production rate in this part of the analysis. The probability for observing the number of events seen in each bin for an expectation of n_k is calculated using Poisson statistics. The statistical fluctuations in c_{ki} and $\sigma_k^{\rm bkg}$ are taken into account using the method of [25]. The negative $\log L$ distributions for each of the α parameters studied are shown in Fig. 2.

The information given by the observed event rates is included by calculating the likelihood for the mean number of events expected as a function of α to have resulted in the observed number of events given in the upper part of Table 1. This is calculated separately for each channel. The variation of the mean number of signal events expected as a function of α is determined using fully simulated EXCALIBUR events subjected to the same selection requirements as the data. The number of selected events is parameterised using the quadratic dependence mentioned earlier. The overall normalisation is adjusted to agree with the GENTLE prediction at the Standard Model point. The probability of finding the observed number of events is calculated assuming a Poisson distribution for the signal and background in each channel. The probabilities obtained for each channel are multiplied together and the negative $\log L$ distribution obtained. These are shown in Fig. 2 for each parameter considered.

The curves due to the total and differential cross-section information are consistent with each other for each of the α parameters. Both curves provide a useful constraint. These are independent measurements and are added together to give the overall $\log L$ distributions shown as the dash-dotted lines in Fig. 2.

We also calculate the two dimensional likelihood distributions resulting when two anomalous couplings are simultaneously allowed to vary from the Standard Model. This is incorporated into both parts of the analysis described above by parameterising the predicted variation of signal events using a quadratic function of both TGCs. The resulting 95% probability contours for different pairs of couplings are shown in Fig. 3. We also perform the analysis allowing all three of the α parameters to vary simultaneously. The resulting set of two dimensional correlation contours are also shown in Fig. 3a, b and c, where in each case the third parameter is varied in order to re-minimise the $\log L$ at each point in the two dimensional space.

Alternative analyses

We have developed two other independent analyses, which are largely complementary. The first method uses a simple unbinned maximum likelihood approach which does not include the effects of Γ_W, ISR, acceptance, resolution or background in the analysis of the kinematic vari-

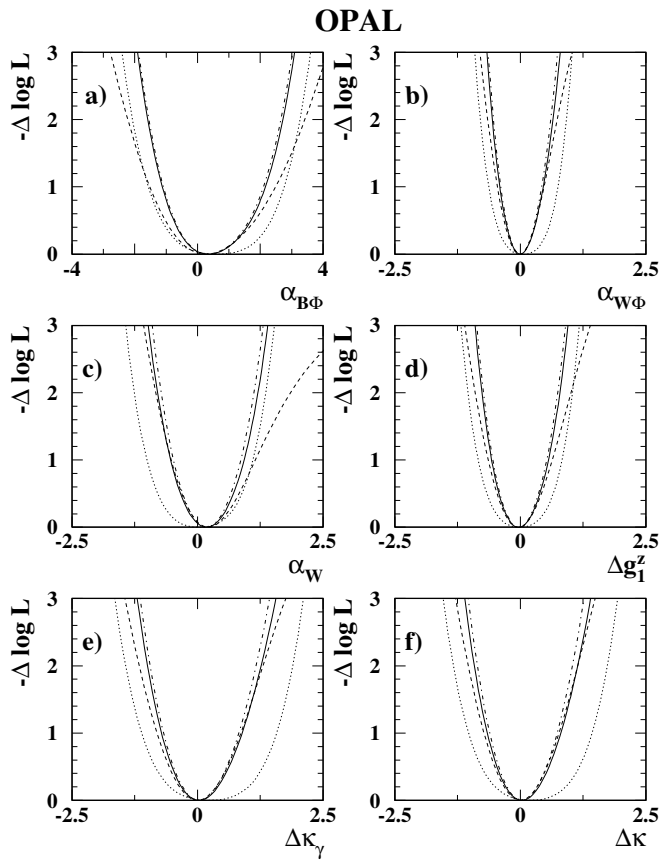

Fig. 2. The negative log likelihood curves (statistical contribution only) obtained from the total event rate (*dotted*) and the shape of the differential distributions (*dashed*). The *dot-dashed curve* is obtained by adding these together. The *solid curve* shows the final result obtained when the systematic error is added. The Δ prefix indicates that the likelihood is shown relative to its minimum value. The figures correspond to **a** $\alpha_{B\phi}$, **b** $\alpha_{W\phi}$, **c** α_W, **d** Δg_1^z, **e** $\Delta\kappa_\gamma$ assuming the HISZ constraints and **f** $\Delta\kappa$ assuming $\Delta\kappa_\gamma = \Delta\kappa_z$

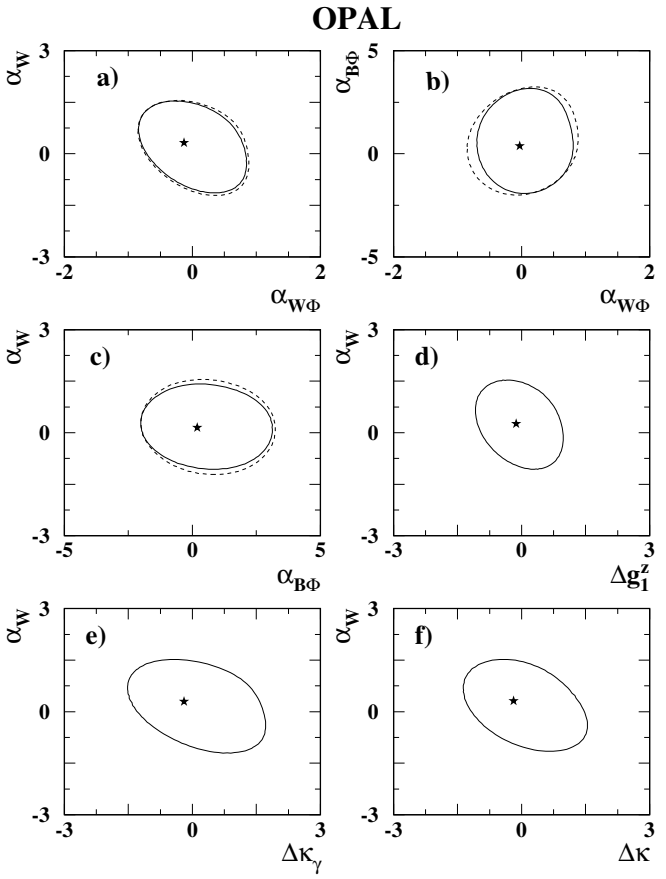

Fig. 3. The 95% C.L. two dimensional correlation contours for different TGC parameters. The effect of statistical and systematic errors is included. The *star* indicates the minimum point. The first three plots show all pairs of the $\alpha_{B\phi}$, $\alpha_{W\phi}$, and α_W parameters. Figure **d** shows Δg_1^z-vs-α_W, Fig. **e** shows $\Delta\kappa_\gamma$-vs-α_W assuming the HISZ constraints and Fig. **f** shows $\Delta\kappa$-vs-α_W assuming $\Delta\kappa_\gamma = \Delta\kappa_z$. In Figs. **a**, **b** and **c** the *dashed line* shows the results obtained by varying all three α parameters (see text), where both statistical and systematic errors are included

ables. These effects are expected to be small in comparison to the present level of statistical precision, and so the method provides a robust systematic comparison. The second method uses an optimal observables method [26,27] which includes all detector effects. The $\log L$ curves produced by all three methods agree very well and give us confidence in the stability of the results.

5 Systematic error studies

In the $W^+W^- \to q\bar{q}\ell\bar{\nu}_\ell$ channel, we obtain information about the production and decay angles from jet vectors. Jet reconstruction has been studied and tuned extensively at LEP1, showing good agreement between distributions measured from data and Monte Carlo samples. We therefore expect this to be adequate for the small number of events in this sample. Studies of back-to-back jet pairs using the LEP1 data yield the following possible differences between data and the Monte Carlo simulation of jets; 10% for energy resolution, 0.5% for energy scale and 10% for resolution in $\cos\theta$ and ϕ.

As a direct test of $\cos\theta_W$ reconstruction we have used radiative $Z^0 \to q\bar{q}$ events taken from the $\sqrt{s} = 91$, 161 and 172 GeV data. By selecting events containing observed radiated photons with energies up to 20 GeV we obtain a sample of jet pairs exhibiting a similar acollinearity distribution to W decays. Assuming that no other photons have been radiated in the event the true direction of the $Z^0 \to q\bar{q}$ system is opposite to that of the photon and the difference between the value of $\cos\theta$ measured from the photon and that measured from the hadronic system is therefore strongly related to the resolution of $\cos\theta_W$. The results obtained from both data and Monte Carlo events agree well showing no significant differences in shape or width of the distributions. We obtain a conservative upper limit upon the possible relative shift on $\cos\theta_W$ between data and Monte Carlo of 0.01. All of these variations are

then used to vary the Monte Carlo jet reconstruction in the analysis and the resulting changes caused to the TGCs were added in quadrature and taken as a systematic error. These are shown in Table 3 labelled as a).

We have evaluated the systematic errors due to several other factors.

b) The effect of limited Monte Carlo statistics.
c) The uncertainty in the world average measured W mass and the LEP beam energy.
d) The uncertainties of the overall normalisation (selection efficiency and luminosity) given in [15] used in the calculation of the $\log L$ curve derived from the event rate.
e) We have varied the Monte Carlo generator to use both EXCALIBUR and KORALW [28] to generate the Standard Model sample. We have varied the fragmentation model by using HERWIG [29].
f) We have varied the backgrounds within the estimated systematic errors given in [15] in the calculation of the $\log L$ curve derived from the observed event rate. We have doubled and removed the Z^0/γ and two-photon background additions used in the calculation of the $\log L$ curve derived from the differential distributions.
g) The analysis was carried out using Monte Carlo samples generated at a nominal energy of 171 GeV. We have estimated the possible bias this introduces by using Monte Carlo samples generated at 172 GeV as test data.

The errors due to these sources are listed in Table 3.

This analysis relies upon EXCALIBUR correctly describing the variation of cross section, angular distribution and four-fermion background as functions of anomalous TGCs. We have investigated the limits of this assumption by comparing these quantities to those predicted by several other programs (GENTLE, KORALW and ERATO [30]). We find that the total cross section predictions agree to within approximately 2.5% across a wide range of anomalous TGC values and we add this variation as a further systematic error to d). We find that both the angular distributions and the contributions of diagrams in addition to the three W^+W^- diagrams are also compatible between the programs at the level of a few percent and we assign no extra systematic error.

Finally we consider possible biases of the method. This method allows for all effects of Γ_W, ISR, acceptance and detector resolution in the calculation of both $\log L$ curves and is therefore in principle free from biases due to these effects. However biases may be introduced by the coarse binning, by the approximation in the correction used to include detector effects, or by the neglect of the small four fermion background. To quantify these effects we perform the analysis using samples of approximately 20,000 fully simulated four fermion Monte Carlo events produced by both grc4f and EXCALIBUR as input. These samples were generated with different TGC values. In all cases the TGC value reconstructed by the analysis is found to be consistent with the generated value and no significant difference was observed between the grc4f and EXCALIBUR samples. The greater of the statistical precision of the test or the measured bias was taken as a conservative systematic error and is shown in row h) of Table 3.

All contributions to the systematic errors are summarised in Table 3. To include the systematic error in the likelihood curves, we apply a simple procedure which would be exact if all errors were Gaussian. We calculate a function of α, $\Delta \log L(\alpha)_{syst}$, to add to the $\log L$ curves. This is given by

$$\Delta \log L(\alpha)_{syst} = (\alpha - \alpha_0)^T [(V_{stat} + V_{syst})^{-1} - (V_{stat})^{-1}](\alpha - \alpha_0)$$

where α represents a vector of one or more TGC parameters, α_0 is the TGC value at the minimum of the $\log L$ curve, V_{syst} is the systematic error matrix constructed assuming the errors are Gaussian, and V_{stat} is approximated (for this purpose only) by assuming a parabolic $\log L$ distribution around α_0. The full $\log L$ curves for each parameter are obtained by adding $\Delta \log L(\alpha)_{syst}$ to the $\log L$ curve due to statistical errors only, and these are shown as solid lines in Figs. 2 and 3

6 Results and conclusion

We express the results as measurements with the one standard deviation limits given by the values of α where the negative $\log L$ curve rises by 0.5 from the minimum. The results are given in Table 4 where the statistical and systematic errors are shown separately. The expected statistical errors for a sample of this size were evaluated by repeating the analysis using Monte Carlo events divided into sub-samples equivalent to the actual data sample. The RMS spread and the average error agreed within 10%, and the latter is shown in the table.

We also express the results as 95% confidence level (C.L.) limits given by the values of α where the change in likelihood is 1.92. The ranges obtained are shown in Table 4.

In our previous publication [3] we have presented a measurement of the $\alpha_{W\phi}$ parameter using the 161 GeV data. By including the $\log L$ obtained from that measurement in this analysis we obtain the combined result $\alpha_{W\phi}=-0.08^{+0.28}_{-0.25} \pm 0.10$. The corresponding 95% C.L. range is $-0.59 < \alpha_{W\phi} < 0.52$.

The results which we have obtained for the parameters listed as c), e) and f) in the results table can be compared with those reported recently by CDF [1] and D0 [2] which are a factor of between two and three more precise. The measurements agree in all cases.

In conclusion, we have presented results using W^+W^- events reconstructed from $10.4\,\mathrm{pb}^{-1}$ of data recorded at LEP2 at a centre-of-mass energy of 172 GeV. We have used the observed W^+W^- event rate and the distribution of kinematic variables to place limits upon possible anomalous triple-gauge-boson couplings. We measure $\alpha_{B\phi}=0.35^{+1.29}_{-1.07} \pm 0.38$, $\alpha_{W\phi}=0.00^{+0.30}_{-0.28} \pm 0.11$, $\alpha_W = 0.18^{+0.49}_{-0.47} \pm 0.23$, $\Delta g_1^z=-0.03^{+0.40}_{-0.37} \pm 0.14$, $\Delta\kappa_\gamma^{(HISZ)} = 0.03^{+0.55}_{-0.51} \pm 0.20$, and $\Delta\kappa=0.03^{+0.49}_{-0.46} \pm 0.21$. These results

Table 3. Contributions to the systematic errors in the determination of TGC parameters

	Source	Error on parameter					
		$\alpha_{B\phi}$	$\alpha_{W\phi}$	α_W	Δg_1^z	$\Delta\kappa_\gamma$	$\Delta\kappa$
a)	Jet reconstruction	0.21	0.05	0.03	0.05	0.12	0.12
b)	MC statistics	0.06	0.04	0.05	0.05	0.06	0.07
c)	W mass/LEP energy	0.04	0.01	0.01	0.00	0.01	0.01
d)	Overall normalisation	0.07	0.01	0.02	0.01	0.02	0.02
e)	MC generator	0.11	0.02	0.15	0.02	0.04	0.08
f)	Background	0.22	0.06	0.12	0.06	0.11	0.09
g)	171/172 GeV diff.	0.12	0.05	0.10	0.08	0.07	0.07
h)	Bias tests	0.11	0.04	0.05	0.05	0.06	0.06
	Total	0.38	0.11	0.23	0.14	0.20	0.21

Table 4. Measurements of anomalous coupling parameters using the OPAL 172 GeV data sample. The measured values and one standard deviation errors are shown in column 2, where the statistical (asymmetric) and systematic (symmetric) errors are shown separately. The expected error obtained from multiple Monte Carlo samples is shown in the third column. The 95% confidence level ranges including systematic errors are shown in the fourth column

Parameter	Measurement	Expected stat. err.	95% C.L. range
$\alpha_{B\phi}$	$0.35^{+1.29}_{-1.07} \pm 0.38$	± 1.1	$[-1.6, 2.7]$
$\alpha_{W\phi}$	$0.00^{+0.30}_{-0.28} \pm 0.11$	± 0.29	$[-0.55, 0.64]$
α_W	$0.18^{+0.49}_{-0.47} \pm 0.23$	± 0.48	$[-0.78, 1.19]$
Δg_1^z	$-0.03^{+0.40}_{-0.37} \pm 0.14$	± 0.39	$[-0.75, 0.77]$
$\Delta\kappa_\gamma^{(HISZ)}$	$0.03^{+0.55}_{-0.51} \pm 0.20$	± 0.53	$[-0.98, 1.24]$
$\Delta\kappa_\gamma = \Delta\kappa_z$	$0.03^{+0.49}_{-0.46} \pm 0.21$	± 0.50	$[-0.90, 1.12]$

agree with the Standard Model expectation of zero for each anomalous coupling. The negative $\log L$ distributions for these parameters are shown in Fig. 2. The two dimensional correlation contours are shown in Fig. 3.

Acknowledgements. We particularly wish to thank the SL Division for the efficient operation of the LEP accelerator at all energies and for their continuing close cooperation with our experimental group. We thank our colleagues from CEA, DAPNIA/SPP, CE-Saclay for their efforts over the years on the time-of-flight and trigger systems which we continue to use. In addition to the support staff at our own institutions we are pleased to acknowledge the Department of Energy, USA, National Science Foundation, USA, Particle Physics and Astronomy Research Council, UK, Natural Sciences and Engineering Research Council, Canada, Israel Science Foundation, administered by the Israel Academy of Science and Humanities, Minerva Gesellschaft, Benoziyo Center for High Energy Physics, Japanese Ministry of Education, Science and Culture (the Monbusho) and a grant under the Monbusho International Science Research Program, German Israeli Bi-national Science Foundation (GIF), Bundesministerium für Bildung, Wissenschaft, Forschung und Technologie, Germany, National Research Council of Canada, Hungarian Foundation for Scientific Research, OTKA T-016660, T023793 and OTKA F-023259.

References

1. CDF Collaboration, F. Abe et al., Phys. Rev. Lett. **75** (1995) 1017; CDF Collaboration, F. Abe et al., Phys. Rev. Lett. **78** (1997) 4536
2. D0 Collaboration, S. Abachi et al., Phys. Rev. Lett. **75** (1995) 1023; S. Abachi et al., Phys. Rev. Lett. **75** (1995) 1034; S. Abachi et al., Phys. Rev. Lett. **77** (1996) 3303; S. Abachi et al., Phys. Rev. Lett. **78** (1997) 3634; S. Abachi et al., Fermilab-Pub-97/088-E, submitted to Phys. Rev. D; B. Abbott et al., Phys. Rev. Lett. **79** (1997) 1441
3. OPAL Collaboration, K. Ackerstaff et al., Phys. Lett. **B397** (1997) 147
4. DELPHI Collaboration, P. Abreu et al., Phys. Lett. **B397** (1997) 158; L3 Collaboration, M. Acciarri et al., Phys. Lett. **B398** (1997) 223
5. L3 Collaboration, M. Acciarri et al., CERN-PPE/97-98, submitted to Phys. Lett. B
6. Physics at LEP2, Edited by G. Altarelli, T. Sjostrand, F. Zwirner, Report on the LEP2 workshop 1995, CERN 96-01 (1996) Vol. 1, 525
7. K. Hagiwara, R.D. Peccei, D. Zeppenfeld, K. Hikasa, Nucl. Phys. **B282** (1987) 253
8. M. Bilenky, J.L. Kneur, F.M. Renard, D. Schildknecht, Nucl. Phys. **B409** (1993) 22; M. Bilenky, J.L. Kneur, F.M. Renard, D. Schildknecht, Nucl. Phys. **B419** (1994) 240
9. K. Gaemers, G. Gounaris, Z. Phys. **C1** (1979) 259
10. A. De Rujula, M.B. Gavela, P. Hernandez, E. Masso, Nucl. Phys. **B384** (1992) 3
11. K. Hagiwara, S. Ishihara, R. Szalapski, D. Zeppenfeld, Phys. Lett. **B283** (1992) 353, Phys. Rev. **D48** (1993) 2182
12. LEP Energy Working Group, LEP energy calibration in 1996, LEP Energy Working Group Internal note 97-01
13. The OPAL Collaboration, K. Ahmet et al., Nucl. Instr. Meth. **A305** (1991) 275; P.P. Allport et al., Nucl. Instr. Meth. **A324** (1993) 34; P.P. Allport et al., Nucl. Instr. Meth. **A346** (1994) 476
14. B.E. Anderson et al., IEEE Transactions on Nuclear Science, **41** (1994) 845

15. OPAL Collaboration, K. Ackerstaff et al., CERN-PPE/97-116, submitted to Eur. Phys. J. C
16. The Particle Data Group, R.M. Barnett et al., Phys. Rev. **D54** (1996) 1; CDF Collaboration, F. Abe et al., Phys. Rev. Lett. **75** (1995) 11, Phys. Rev. **D52** (1995) 4784; CDF Collaboration, F. Abe et al., Phys. Rev. Lett. **65** (1990) 2243, Phys. Rev. **D43** (1991) 2070; UA2 Collaboration, J. Alitti et al., Phys. Lett. **B276** (1992) 354; UA1 Collaboration, C. Albajar et al., Z. Phys. **C44** (1989) 15
17. D. Bardin et al., Nucl. Phys. B, Proc. Suppl. **37B** (1994) 148-157
18. J. Allison et al., Nucl. Instr. Meth. **A317** (1992) 47
19. N. Brown, W.J. Stirling, Phys. Lett. **B252** (1990) 657; S. Bethke, Z. Kunszt, D. Soper, W.J. Stirling, Nucl. Phys. **B370** (1992) 310; S. Catani et al., Phys. Lett. **B269** (1991) 432; N. Brown, W.J. Stirling, Z. Phys. **C53** (1992) 629
20. The OPAL Collaboration, M.Z. Akrawy et al., Phys. Lett. **B253** (1990) 511
21. T.Sjöstrand, Comp. Phys. Comm. **82** (1994) 74
22. J. Fujimoto et al., KEK-CP-046, Comp. Phys. Comm. **100** (1997) 128
23. F.A. Berends, R. Pittau, R. Kleiss, Comp. Phys. Comm. **85** (1995) 437; F.A. Berends, A.I. van Sighem, Nucl. Phys. **B454** (1995) 467
24. R.L. Sekulin, Phys. Lett. **B338** (1994) 369
25. R. Barlow, C. Beeston, Comp. Phys. Comm. **82** (1994) 74
26. M. Diehl, O. Nachtmann, Z. Phys. **C62** (1994) 397
27. C.G. Papadopoulos, Phys. Lett. **B386** (1996) 442
28. M. Skrzypek et al., Comp. Phys. Comm. **94** (1996) 216; M. Skrzypek et al., Phys. Lett. **B372** (1996) 289
29. G. Marchesini et al., Nucl. Phys. B, Comp. Phys. Comm. **67** (1992) 465
30. C. Papadopolous, Comp. Phys. Comm. **101** (1997) 183